Polym. Bull. (2015) 72:1095–1112
DOI 10.1007/s00289-015-1325-4

ORIGINAL PAPER

Thermal stability and thermal degradation kinetics (model-free kinetics) of nanocomposites based on poly (lactic acid)/graphene: the influence of functionalization

Pedram Manafi · Ismaeil Ghasemi · Mohammad Karrabi · Hamed Azizi · Mohammad Reza Manafi · Parvin Ehsaninamin

Received: 26 June 2014 / Revised: 24 January 2015 / Accepted: 2 February 2015 /
Published online: 10 February 2015

Abstract Thermal stability and thermal degradation kinetics of nanocomposites play an important role in many applications. In this study, nanocomposites based on poly (lactic acid) (PLA)/graphene containing 0.5 and 1 wt% were prepared via solution method. Functionalized graphene were prepared by acid treatment followed by grafting PLA on their surfaces. The functionalized graphene was characterized using fourier transform infrared spectroscopy (FTIR), Raman, elemental analysis, Fourier transform infrared attenuated total reflection (FTIR-ATR), Dynamic mechanical thermal analysis (DMTA) and thermogravimetry analysis (TGA). The results revealed a successful functionalization reaction. The morphology of nanocomposites was investigated by scanning electron microscopy (SEM). Thermal kinetics of samples was studied using TGA in multiple heating rates (5, 10, 20 and 30 °C/min). Flynn–Wall–Ozawa (FWO) and Vyazovkin (VYZ) methods were considered as isoconversional models. Although the assumptions of the applied models were different, there was a good agreement between the models and obtained activation energies.

Keywords Polymers · Nanostructures · Thermal properties · Thermogravimetry analysis

P. Manafi · I. Ghasemi (✉) · M. Karrabi · H. Azizi
Plastic Department, Iran Polymer and Petrochemical Institute, P.O.Box: 14965/115, Tehran, Iran
e-mail: i.ghasemi@ippi.ac.ir

M. R. Manafi
Department of Applied Chemistry, Islamic Azad University, South Tehran Branch, Tehran, Iran

P. Ehsaninamin
Faculty of Chemistry, Tehran North Branch of Islamic Azad University, Tehran, Iran

Introduction

Due to their desirable features including sustainability, eco-friendly and biodegradability, poly (lactic acid) (PLA) has been attractive in polymer industries as a new class of materials. PLA can be a suitable candidate to use in packaging, fibers, membranes, tissue engineering, automotive parts and electrical devices. To broaden the application of PLA, tailoring its properties has been considered by researchers [1–5]. Copolymerization and compounding with other polymers and additives are the two main strategies for modification of PLA properties. In addition, many attempts have been focused on incorporation of low amounts of nanoparticles into the PLA matrix. Among different types of nanoparticles, graphene nanoplatelets (GNp) show unique properties and can improve mechanical, electrical and thermal properties of PLA [6–8].

GNp can be a good alternative for conductive carbon fillers in nanocomposites, due to its high aspect ratio, easy production and excellent conductivity. The enhancement of mechanical, physical, thermal and barrier properties in nanocomposites containing graphene has been reported in the literatures [9–12]. Uniform dispersion of fillers plays the main role in the improvement of physical and mechanical properties. Due to mismatching and nature of graphene with most polymers, a good dispersion has not been obtained thus functionalization is an inevitable process. In comparison with non-functionalized GNp, functionalized graphene nanoplatelets (FGNp) have many oxygen-containing groups on their surfaces. These functional groups not only provide proper dispersion of FGNp in polymers, but also facilitate the interaction between the matrices and FGNp through covalent bonds. The first step in functionalization is oxidation using acid treatment. Characterization of oxidized graphene has revealed that existence of epoxide and hydroxyl groups at the surface of the FGNp together with carbonyl and carboxyl groups located at the edges enables the nanoplatelets to be readily grafted with different groups. Grafting of various functional groups such as ester and amine is the second step and has usually been carried out using acylation reaction [13, 14].

Kinetic study of the thermal degradation can be used to assess the reliability of the materials for high-temperature applications. The triplet kinetic parameters such as activation energy (E_a), pre-exponential factor (A) and reaction model (n) of thermal degradation of polymers give useful information about the decomposition mechanism [15]. To calculate the kinetic parameters, the International Confederation of Thermal Analysis and Calorimetry (ICTAC) insisted on using the multiple heating rate processes, then avoided single heating rate methods and later suggested some recommendations for performing kinetic computations on thermal analysis data [16]. Conversion function ($f(\alpha)$) and the activation energy have been determined via the various methods. Generally, these methods can be divided into two categories: I. isoconversional and II. model-fitting methods. Isoconversional method can be explained as model-free method in which there are no changes of conversion function with the variation of the heating rate for whole ranges of the degree of conversion (α).

To determine the kinetic triplets using multiple heating rate tests, model-fitting kinetic methods can be used. In this method, the obtained data for non-isothermal

condition are not comparable with those of isothermal condition [17, 18]. One of the best free approaches is Vyazovkin model through use of isoconversion method leads to an authentic way of obtaining kinetic information from non-isothermal data using thermal analysis.

Thermal degradation kinetics of nanocomposites based on biodegradable polymers has gained an important role in processing and applications at high temperatures. Effect of carbon nanotube, functionalized carbon nanotube, hydroxyapatite, calcium carbonate and graphene on kinetics of degradation has been studied by researchers [19–23]. Kim et al. reported the effect of calcium carbonate on the thermal degradation kinetics of PLA/calcium carbonate nanocomposites by different models. They revealed that the activation energy of nanocomposite samples was lower than that of neat PLA due to the basic nature of calcium carbonate and its catalytic effect on depolymerization of the PLA ester bonds [21]. The similar results have been reported by Barrosso-Bujans et al. for the nanocomposites based on polyethylene oxide/graphene. They attributed this trend to the linear structure of polyethylene oxide and showed that thermal degradation follows the first-order reaction [22]. The contradictory result has been reported by Chrissafis for PLA/oxidized multiwalled carbon nanotube in which the nanocomposite samples had higher activation energy compared to neat PLA. He believed that the presence of a complex degradation mechanism (more than two mechanisms) was the main reason for this difference [19].

This work is motivated by current researches in the thermal degradation kinetics of nanocomposites. We reported the functionalization of GNp and preparation of PLA/GNp and FGNp nanocomposites. The functionalization reaction was tracked by FTIR, thermogravimetry analysis (TGA), Raman and elemental analyses. The nanocomposites samples were prepared via solution method. Thermal stability and degradation kinetics were studied based on TGA data. For the first time, thermal degradation kinetics was evaluated using model-free kinetic methods for grafted nanocomposites. The two model-free kinetic methods (VYZ and FWO) are used to compare and evaluate the activation energies and the results were discussed.

Experimental

Materials

Poly (lactic acid) (3251D) was purchased from NatureWorks, USA. Graphene nanoplatelets which were prepared via a modified Hummers method (specific surface area 150 m^2/g, length 1.5–2.5 μm, bulk density 0.03–0.1 g/cc, thickness 4–20 nm, layers <30, diameter 5–10 μm, typical value of resistivity: 107 and 102 Ω/m parallel to surface and perpendicular to surface, respectively) were kindly supplied by Research Institute of Petroleum Industry (RIPI), IRAN. Sulfuric acid (98 %), nitric acid (68 %), thionyl chloride ($SOCl_2$), *N*, *N*-dimethylformamide (DMF) and tetrahydrofuran (THF) were purchased from Sigma-Aldrich. THF was dried over sodium benzophenone under nitrogen and freshly distilled prior to use, to obtain better performance.

Graphene functionalization

0.2 g GNp was placed in a vacuum oven about 48 h at 80 °C to remove absorbed humidity. A mixture of H_2SO_4/HNO_3 (3:1, v/v) was used to oxidize the GNp to create carboxylic and hydroxyl functional groups for 2 h using a sonicator (60 °C, 630 W). The oxidized GNp was filtered through a polycarbonate filter (0.45 μm pore diameter), and washed with deionized water several times until the pH value got around 7 and was then dried in a vacuum oven at 80 °C overnight.

In the next step of GNp modification, the acylation reaction was done using a mixture of 20:1 thionyl chloride and dimethylformamide under sonication for 2 h at 70 °C in a N_2 atmosphere. GNp-COCl was filtered through a poly(tetrafluoroethylene) filter (0.45 μm pore diameter), and washed with dried THF to remove residual $SOCl_2$. The obtained GNp-COCl was then dried under vacuum at 40 °C for 24 h and stored in a sealed bottle for further use. The aforementioned steps are shown in Scheme 1.

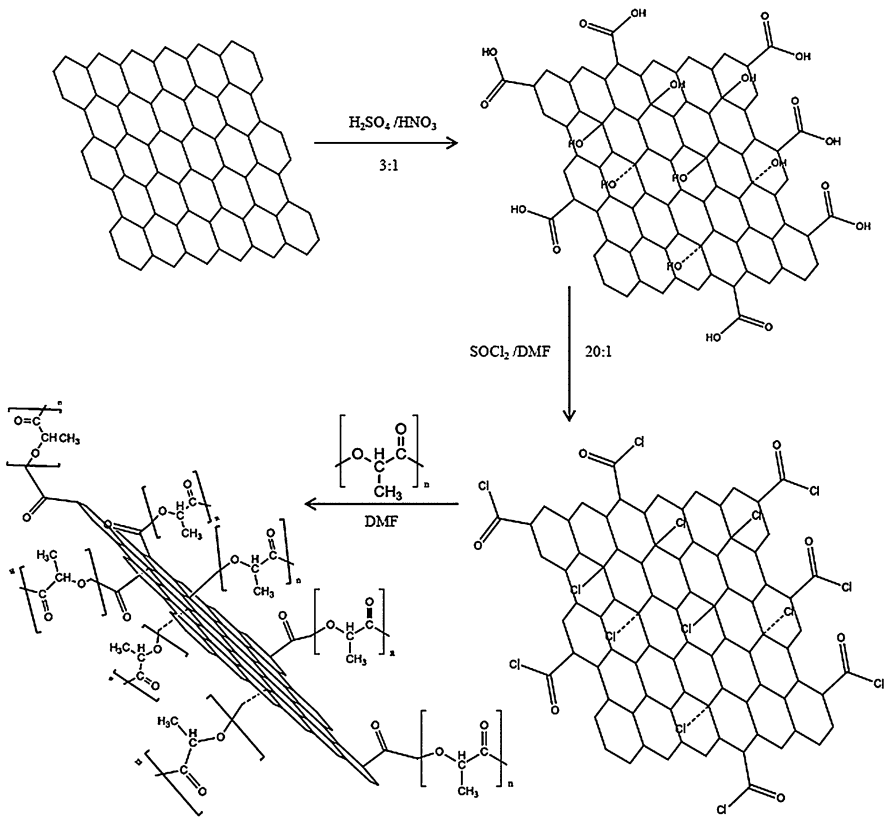

Scheme 1 Different steps of GNp modification

Nanocomposite preparation

The desired amounts of GNp-COCl and GNp were first added into dried DMF at a concentration of 1 mg/ml, and the mixture was sonicated at 630 W for 2 h to obtain a uniform suspension. At the same time, PLA was completely dissolved in dried DMF at a concentration of 100 mg/ml at 45 °C. The PLA solution was then mixed with the GNp-COCl and GNp suspension for 4 h at 40 °C. After further sonication (10 min), the solvent was evaporated at an elevated temperature for about 1 h, and the PLA/GNp and PLA/FGNp nanocomposite films were obtained. The films were further dried at 80 °C in a vacuum oven for 3 days to completely remove the solvent. Then the mixture was washed in DMF (80 °C) to extract the un-reacted PLA until the filtrate would not sediment in system. The concentrations of GNp and FGNp were 0.5 and 1 wt%, and the samples were denoted by PLA/GNp 0.5, PLA/GNP 1, PLA/FGNp 0.5 and PLA/FGNp 1.

Characterization

To characterize the functionalization reaction, FTIR spectra were collected on the Bruker EQUINOX 55 FTIR spectrometer, Ettlingen (collecting 32 scans in the 400–4,000 cm^{-1} range with 4 cm^{-1} resolution). Raman spectra of samples were carried out with an ALMEGA-Dispersive Raman (Thermo Nicolet) with 514.5 nm excitation. Fourier transform infrared attenuated total reflection was used (Specac Golden gate spectrometer). TGA was performed on a Polymer Laboratories model STA 1640 (UK) under nitrogen atmosphere from ambient temperature up to 600 °C at a heating rate of 10 °C/min also used to monitor the modification reaction of GNp. Elemental analysis of samples was performed by Elementar Vario EL III. To study kinetics of thermal degradation, rates of 5, 10, 20 and 30 °C/min in TGA were used. The morphology of nanocomposites was investigated by scanning electron microscopy (SEM, Vega Tescan) before the test, rectangular bars were cryogenically fractured in liquid nitrogen carefully and then the samples were coated with gold. Dynamic mechanical thermal analysis (DMTA) was performed using a Tritec 2000 DMA instrument (Triton Technology, UK) with a chuck distance of 21 mm at temperature range of 30–110 °C, heating rate of 3 °C/min and frequency of 1 Hz. All the samples were tested in the single cantilever bending mode.

Results and discussion

Functionalization of GNp

To monitor functionalization reaction of GNp, FTIR analysis was conducted. Figure 1 shows FTIR spectra of GNp and FGNp. As can be seen, the peaks at 1,707, 1,580 and 1,130 cm^{-1} are appeared in the spectra of FGNp, which reflected the formation of carbonyl groups [from carboxylic acids (–COOH–)], asymmetric –COO– stretch and symmetric –COO– stretch, respectively. In spite of existence of a small peak at 3,433 cm^{-1} which corresponds to hydroxyl groups in GNp, the peak

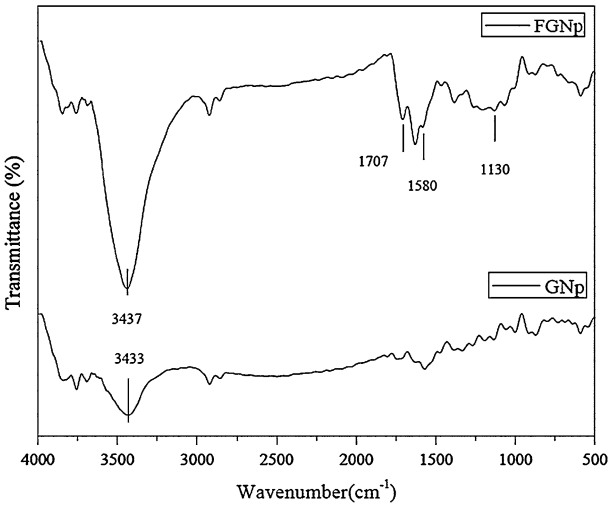

Fig. 1 FTIR spectra of GNp and FGNp

was significantly strengthened after the acid treatment. Similar results about carbon nanotube functionalization have been reported [24, 25] and the FTIR spectra confirm that acid treatment produces oxygen-containing functional groups on the surface of GNp.

Another useful and powerful method for characterization of functionalization reaction of GNp is Raman spectroscopy. The Raman spectra of GNp and FGNp are demonstrated in Fig. 2. As it was expected, two sharp peaks are detectable in the spectrum of carbon allotropes, which are known as D and G bands. The D band appears around 1,340-1,360 cm^{-1} which is attributed to the ring breathing modes of sp^2 atoms in rings. The G band is an indication of bond stretching of all pairs of sp^2 atoms in both rings and chains and appears around 1,585 cm^{-1} [26]. On the other hand, the main characteristics peaks for PLA are appeared in 1,728, 1,402, 1,242, 1,064 and 976 cm^{-1} and there are no overlaps between the graphene and PLA in the range of 1,300–1,500 cm^{-1}.

The intensity ratio of D and G band (I_D/I_G) is affected by the disordered pattern which exists in graphene platelets and is different for pristine and functionalized graphene due to the formation of defects in FGNp. The ratios were 1.15 and 1.39 for GNP and FGNP, respectively. The increase of I_D/I_G ratio in FGNp implies a successful functionalization reaction [27].

The next analysis for tracking GNp functionalization was TGA. TGA curves of GNp and FGNp are shown in Fig. 3. There are two major mass loss steps while increasing the temperature of GNp sample. The mass loss around 100 °C is assigned to the removal of absorbed water and release of moisture, and the other one around 200 °C is due to the pyrolysis of the liable oxygen-containing functional groups [28]. In the range of 150–230 °C, the mass losses were 3 and 8 wt% for GNp and FGNp, respectively. The different thermal behavior of the samples may be

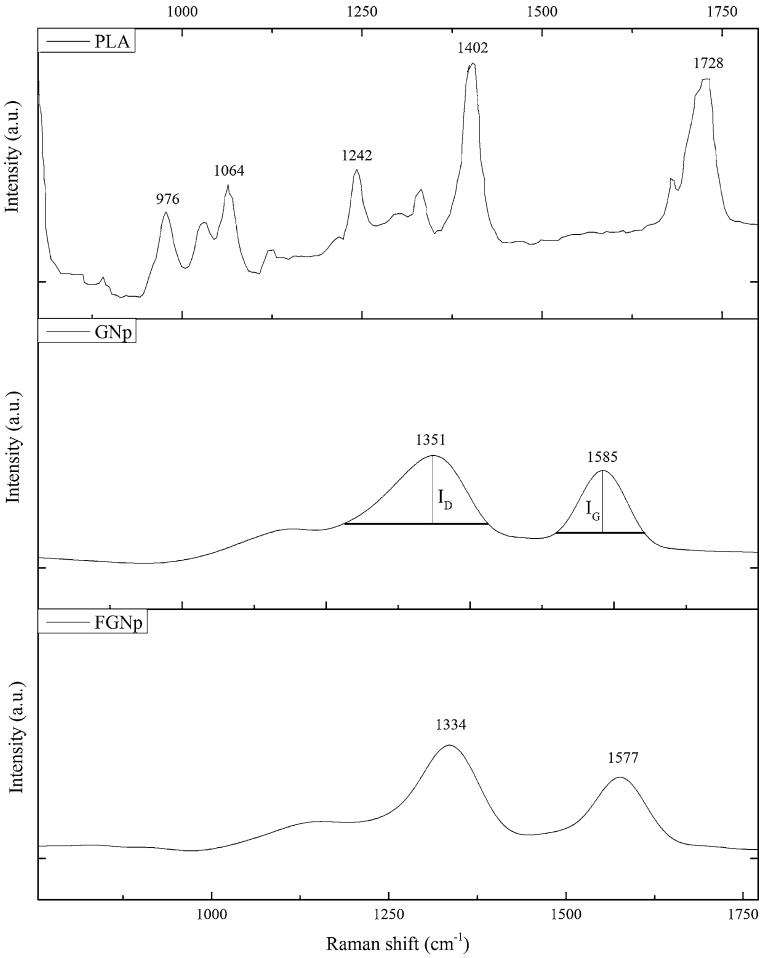

Fig. 2 Raman spectra of PLA, GNp and FGNp

attributed to the presence of oxygen-containing groups on the surface of FGNp. In other meaning, in this temperature range, due to the existence of more organic groups which are formed by acid treatment, the mass loss is more significant than that of GNp.

The results of elemental analysis are listed in the Table 1. As it can be seen, the oxygen percentage of FGNp is increased due to the formation of oxygen-containing groups by acid treatment.

Grafting FGNp to PLA

Grafting reaction of PLA on FGNp was also monitored by FTIR-ATR analysis. Figure 4 represents the FTIR–ATR spectra for samples of PLA, PLA/GNp 1 and PLA/FGNp 1 nanocomposites. The spectra depicted all of the important

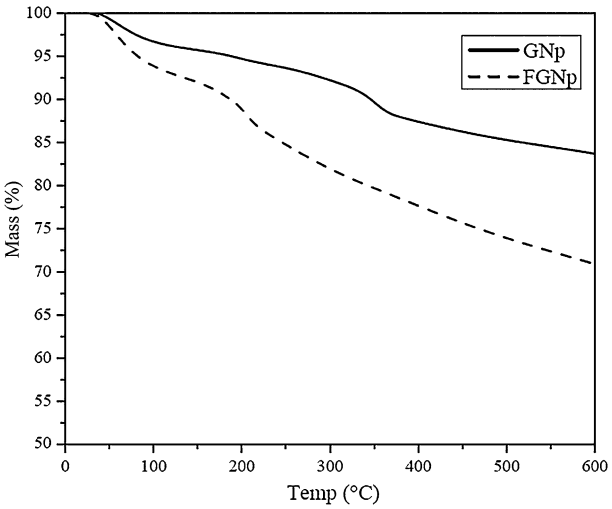

Fig. 3 TGA curve of GNp and FGNp

Table 1 Elemental analysis of GNp and FGNp

Sample	C (%)	O (%)
GNp	87.08	5.39
FGNp	80.13	11.25

characteristic bonds associated with PLA and the most obvious differences are in variation of intensity and shifting of the bonds. The ester–(COO)– stretching bond for PLA, PLA/GNp 1 and PLA/FGNp 1 was appeared at 1,761, 1,751 and 1,748 cm^{-1}, respectively. It seems that the blue shifting of bonds in samples owes to physical grafting of PLA chains onto the GNp and FGNp. In other words, physical grafting of PLA on the surface of graphene leads to shifting of –(COO)– stretching bond to the lower range wave numbers.

Figure 5 depicts the storage modulus and loss factor (tan δ) of the sample. The glass transitions of the samples were calculated from slope of storage modulus (according to ASTM E1640) and depicted in Table 2. As can be seen, the glass transitions of the samples have shifted to higher temperatures due to presence of the nanoparticles. In addition, Tg of the samples containing FGNp are shifted to higher temperatures due to better interaction with the matrix. In other words, grafting reaction between FGNp and PLA matrix slowed down the movement of the chains and increased *T*g.

Morphology

SEM micrographs of neat PLA and nanocomposites containing GNp and FGNp are shown in Fig. 6. The pure PLA is characterized with smooth fractured surface without any orientation. By the addition of GNp, the fracture surface clearly reveals layered

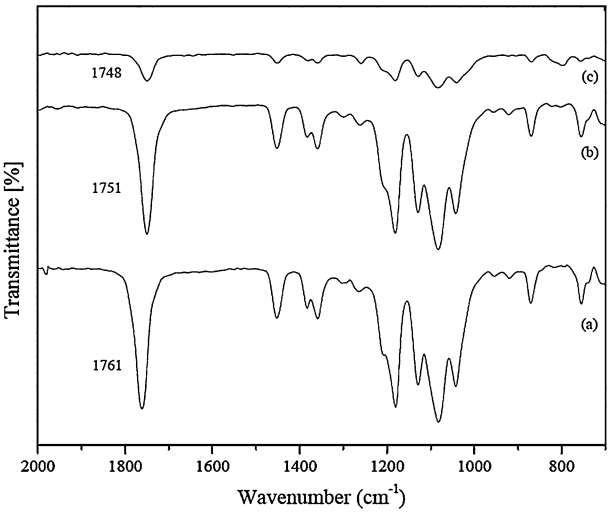

Fig. 4 FTIR-ATR spectra of **a** PLA, **b** PLA/GNp 1 and **c** PLA/FGNp 1

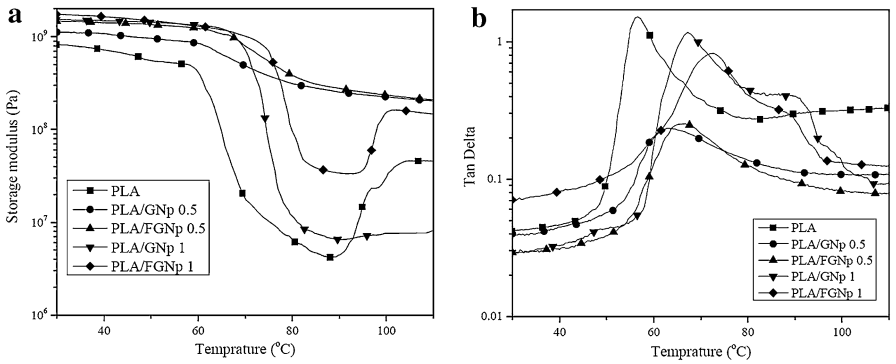

Fig. 5 DMTA of PLA and nanocomposites. **a** Storage modulus and **b** tan δ

structures with uniformly dispersed GNp in PLA matrix. The orientation of graphene may be caused by gravitational forces and also ultrasonic waves experienced by the platelet-like nanosheets. It can be seen that after functionalization of GNp and grafting PLA to FGNp, platelet structure is much pronounced (Fig. 6c, e).This difference may be attributed to the easier and better formation of 2D structure of PLA/FGNP which leads to better dispersion and distribution of fillers into matrix. This phenomenon is shown more clearly in Fig. 6f, g with higher magnification.

Thermal degradation analysis of nanocomposites

Thermal stabilities of nanocomposites were evaluated by TGA. Figure 7 plots the TGA and DTG curves of the samples containing different nanoparticles at 5 °C/min

Table 2 Glass transition temperatures of samples obtained from DMTA

Samples	PLA	PLA/GNp 0.5	PLA/GNp 1	PLA/FGNp 0.5	PLA/FGNp 1
T_g (°C)	58.22	62.16	67.39	65.16	73.53

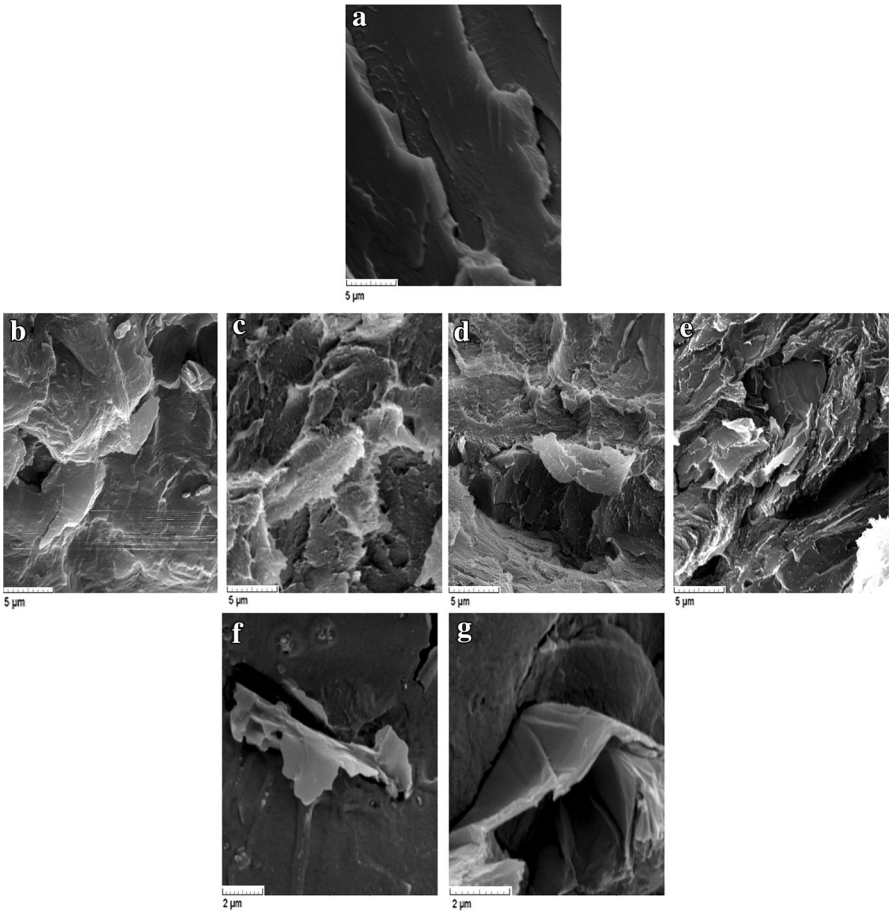

Fig. 6 SEM micrographs of **a** neat PLA, **b** PLA/GNp 0.5, **c** PLA/FGNp 0.5, **d** PLA/GNp 1, **e**, **f**, **g** PLA/FGNp 1

under an atmosphere of nitrogen. To interpret thermal behavior of the samples, the maximum rate of mass loss (T_p) and the onset temperatures of degradation were determined by DTG and TGA, respectively, and are summarized in Table 3. The onset temperatures were determined regarding to their mass loss shapes.

In Table 3, T_p and T_{onset} increased with incorporation of the nanoparticles at the whole range of heating rates. T_p and T_{onset} were shifted to higher temperature with increase in nanoparticles' content because of graphene's thermal stability. The

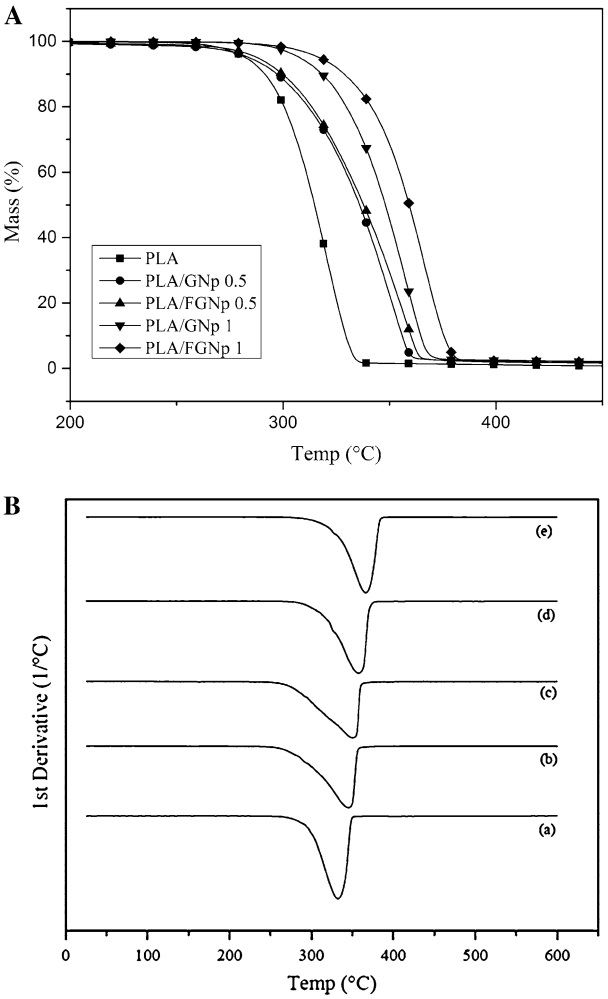

Fig. 7 **A** TGA and **B** DTG curves of *a* neat PLA, *b* PLA/GNp 0.5, *c* PLA/FGNp 0.5, *d* PLA/GNp 1, *e* PLA/FGNp 1 at a heating rate of 5 °C/min

Table 3 T_{onset} and T_p values for PLA and nanocomposites as determined from the TGA and DTG curves

β (°C/min)	T_{onset} (°C)				T_p (°C)			
	5	10	20	30	5	10	20	30
PLA	279	290	307	320	332	356	364	373
PLA/GNp 0.5	285	300	317	329	347	361	380	393
PLA/FGNp 0.5	288	302	320	332	353	363	382	395
PLA/GNp 1	308	321	326	338	358	370	389	398
PLA/FGNp 1	317	325	341	351	365	375	390	400

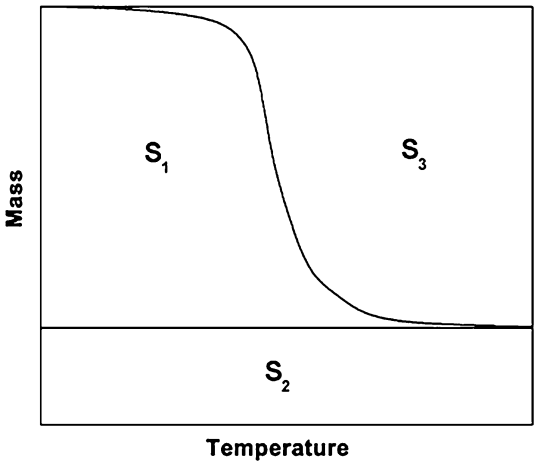

Scheme 2 Representation of S_1, S_2 and S_3 for A^* and K^*

maximum shifting of T_p and T_{onset} to the higher temperatures was attributed to the sample containing 1 wt% of functionalized graphene. Due to the strong interactions between a large numbers of surface atoms of FGNp and PLA molecule chains through C–O–C linkage, the nanoparticles ensnare the movement of the PLA molecule chains. In other words, the modified graphene layers create a shielding on the PLA chains and slow down the decomposition rate of samples. The enhancement of the thermal stability may also result from the barrier effect of FGNp layer structures against the transfer of the thermal decomposition products. These materials have to transfer from a tortuous path and thus the needed temperature for degradation is increased. It can be concluded that T_p and T_{onset} were affected by incorporation of graphene into PLA matrix where they were increased by the increase in nanocontent and functionalization.

The integral procedure decomposition temperature (IPDT) proposed by Doyle involves the volatile parts of the polymeric materials and is used to estimate the inherent thermal stability of the polymeric materials [29–31]. IPDT was calculated as follows:

$$\text{IPDT } (^\circ\text{C}) = A * K * (T_f - T_i) + T_i \quad (1)$$

$$A* = (S_1 + S_2) / (S_1 + S_2 + S_3) \quad (2)$$

$$K* = (S_1 + S_2) / (S_1), \quad (3)$$

where A^* is the area ratio of total experimental TGA thermogram, T_i is the initial experimental temperature, T_f is the final the initial experimental temperature. Scheme 2 shows a representation of S_1, S_2 and S_3 for calculating A^* and K^*.

IPDT of the samples is depicted in Table 4. IPDT of pure PLA was 338.7 °C and the IPDT of nanocomposites was higher than that of pure PLA, which indicates that the filler can improve the thermal stability of PLA.

Table 4 Thermal properties of the samples

Sample	Thermal stability Max thermal degradation rate (1/°C)	IPDT (°C)
PLA	−2.88	338.71
PLA/GNp 0.5	−1.95	548.50
PLA/FGNp 0.5	−2.14	608.57
PLA/GNp 1	−2.46	608.71
PLA/FGNp 1	−2.63	610.91

Thermal degradation kinetics

Decomposition kinetics of polymer using TGA was reported in the ICTAC kinetics committee recommendations for performing kinetic computations on thermal analysis data [16]. Useful data are obtained from this test to determine the decomposition conversion (α), which is defined as:

$$\alpha = \frac{m_0 - m_T}{m_0 - m_{last}}, \tag{4}$$

where m_0, m_T and m_{last} are the initial mass, mass at decomposition temperature and mass at final decomposition reaction, respectively. The most common models, for determination of the activation energy (E_a) in decomposition kinetics, are VYZ and FWO. These models are generally based on Arrhenius equation [32–35].

For non-isothermal conditions, the above equation can be rewritten as:

$$\frac{d\alpha}{dT} = \frac{A}{\beta}\exp\left(\frac{-E_a}{RT}\right)f(\alpha), \tag{5}$$

where α is the conversion (weight of materials volatilized/initial weight of materials), A is the pre-exponential factor, β is the heating rate (°C/min), E_a is activation energy, R is gas constant, $f(\alpha)$ is a function of the fraction of mass or a conversion function of decomposition kinetics and T is temperature.

Flynn–Wall–Ozawa (FWO)

Flynn–Wall–Ozawa model (as the most famous model in non-isothermal conditions) was originated from above equation. Useful parameters such as kinetics triplets [activation energy, pre-exponential factor, function of the fraction $f(\alpha)$] took advantage of applicable parameters, which are able to explain the thermal decomposition kinetics.

The degradation kinetics information (especially activation energy) of Flynn and Wall method was first introduced by Ozawa to form a kinetics model known as the Flynn–Wall–Ozawa (FWO) model. This model was derived from the integral method of Eq. (6) and a linear empirical approximation (given by Doyle [36]) was used. This is applicable to a limited range of $y = E_a/(RT)$ values. The FWO model includes calculating the degradation temperatures corresponding to values of mass loss during the decomposition (α). The Eq. (6) is integrated with $\alpha = 0$ at $T = T_0$

(the initial temperature) and can be assigned using the Doyle approximation [37, 38]. FWO model is expressed in the form of: [34, 39–41]

$$\log \beta = -0.4567(\frac{E_a}{RT}) + (\log(\frac{AE_a}{R}) - \log f(\alpha) - 2.315). \quad (6)$$

According to above equation, at a constant heating rate, E_a can be calculated from the slope of logarithm heating rate as a function of inverse temperature.

Vyazovkin method (VYZ)

Integration of Eq. (5) leads to:

$$g(\alpha) = \int_0^{\alpha} \frac{d\alpha}{f(\alpha)} = A \int_0^{t} \exp(\frac{E_a(\alpha)}{RT})dt = AJ[E_a(\alpha), T], \quad (7)$$

where $g(\alpha)$, $f(\alpha)$ and A are the integral form of the reaction model, the heating program and Arrhenius constant, respectively, and $T(t)$ is also heating program. By considering linear heating rate for $\beta = dT/dt$, $T(t)$ is linear.

Some scientists made the numerical approximations to solve the temperature integrals (I and J) and the results of model-free kinetics (MFK) were significantly different, by the choice of numerical approximations [42, 43]. Vyazovkin and Dollimore proved the fact that for any β, $g(\alpha)$ is constant which can avoid dependence of the numerical approximation. Therefore, with heating rates β_1, β_2 and β_3, three integrals are achieved [$g(\alpha)_{\beta 1} = g(\alpha)_{\beta 2} = g(\alpha)_{\beta 3}$].

$$\frac{A}{\beta_1} I[E_a(\alpha), T]_1 = \frac{A}{\beta_2} I[E_a(\alpha), T]_2 = \frac{A}{\beta_3} I[E_a(\alpha), T]_3 \quad (8)$$

The summary of the equation above is given below:

$$\sum_{i=1}^{n} \sum_{j \neq 1}^{n} \frac{I[E_a(\alpha), T]_i \beta_j}{I[E_a(\alpha), T]_j \beta_i} = 6 \quad \text{for} \quad n = 3\,. \quad (9)$$

From the above equation, activation energy for the samples can be achieved.

The activation energy from kinetics study could be considered as minimum energy for thermal decomposition reaction of the nanocomposites. The slopes of the logarithmic plots of heating rate as a function of inverse temperature were used to calculate the activation energy at stages of degradation based on mass percentage. Figure 8b demonstrates E_a versus different conversions of degradation between 5–90 % of nanocomposite. Significant increment of E_a values could be observed when the specimens were decomposed in the presence of N_2 atmosphere. The differences between activation energies at the initial and later stages of degradations when the specimens were exposed to combusted environment suggest that the specimens have undergone a multistep thermal degradation as shown in Fig. 8b. Two models express the mechanism of degradation of the samples; however, more details can be comprehended from VYZ model-free kinetics (Fig. 8a). VYZ method also

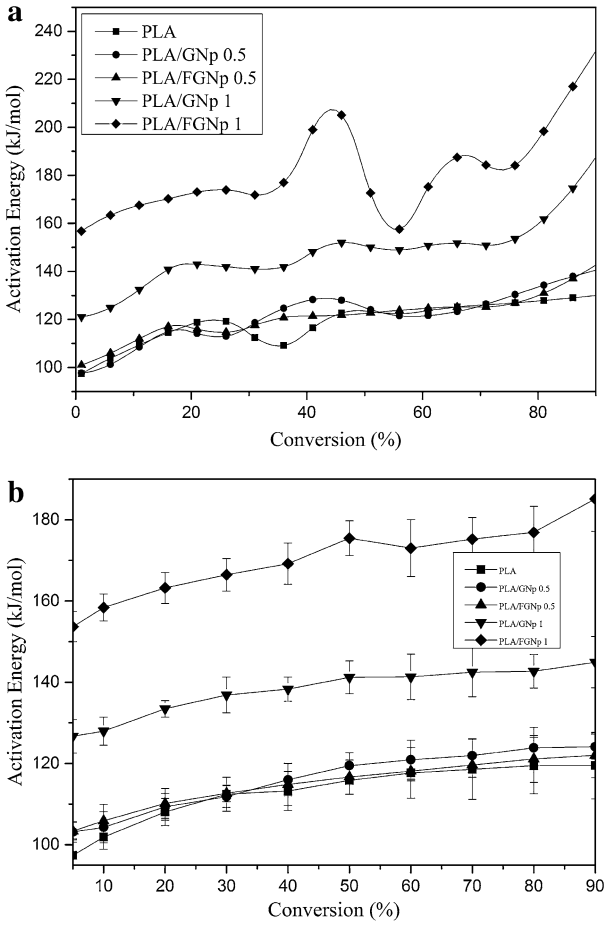

Fig. 8 Activation energies (E_a) for degradation of the samples **a** VYZ method **b** FWO method

suggests that activation energy values for nanocomposites grow with the increase in the conversion. It means that the nanoparticles are well dispersed in the matrix.

In literatures, the mechanism of PLA thermal degradation is complex and consists of random chain scission and unzipping depolymerization reactions [20, 44, 45]. The random degradation reaction includes hydrolysis, oxidative degradation, cis-elimination, intermolecular and intramolecular transesterification. Due to the dependence of activation energy on conversion for neat PLA, there is a competition among random chain scission via cis-elimination and the cyclic rupture via intramolecular transesterification. By the addition of nanoparticles, at the first stage up to 40–50 % of conversion, the same trend was observed which indicates the decomposition obeys from above mechanisms. However, above 50 % conversion, the activation energy was leveled off which means the all mechanisms were shifted to cis-elimination with the lowest energy. In another sense, the presence of graphene

in the compound caused uniform distribution of applied thermal energy and leads to cis-elimination mechanism. The E_a values of FGNp nanocomposites were higher than that of GNp nanocomposite, which could be attended on 2D structure and better effective surface area of the nanocomposites.

It should be noted that the E_a for the thermal degradation of PLA grafted on FGNp (162 kJ/mol) is significantly higher than that of neat PLA (133 kJ/mol). The meaningful difference between E_a for PLA/GNp and neat PLA in this study suggests that polymer–graphene interactions support the rupturing of polymer bonds in pyrolysis conditions. It has been proved that brush-like polymers with long side chains on a substrate can induce natural rupture of covalent bonds in the polymer backbone [46]. This is not really adapted to our case, as PLA has a linear structure and degradation takes place at high temperatures, but it is likely that grafting spreads tension along the nanocomposite and these forces are intensified by the molecular motion resulting from heating.

Conclusions

This study is motivated by current researches in the field of thermal stability and degradation of the nanocomposites. The nanocomposites based on poly (lactic acid)/graphene were prepared via solution method and the effect of functionalization of graphene was studied in thermal degradation kinetics of the samples. The following results can be drawn from this work:

- The oxygen-containing functional groups were induced on the surface of graphene using acid treatment and then characterized by FTIR, Raman, elemental analysis and TGA.
- The grafting reaction of the PLA- and acid-treated nanoparticles was approved by ATR spectra and DMTA analysis.
- SEM micrographs revealed a better dispersion and distribution of nanoparticles with functionalization.
- Multiple heating rates' TGA was applied and activation energies were determined using different models. The results showed that the activation energy for the neat PLA was lesser than those of nanocomposites.
- Samples containing functionalized graphene nanoparticles showed higher activation energies in comparison to samples with unfunctionalized nanoparticles.
- Comparison between two methods (FWO and VYZ) suggests that VYZ method is much more sensitive to thermal degradation kinetics.

References

1. Lunt J (1998) Large-scale production, properties and commercial applications of polylactic acid polymers. Polym Degrad Stab 59(1):145–152
2. Kaplan DL (1998) Biopolymers from renewable resources. Springer, Berlin
3. Drumright RE, Gruber PR, Henton DE (2000) Polylactic acid technology. Adv Mat 12(23):1841–1846

4. Tsuji H, Fukui I (2003) Enhanced thermal stability of poly (lactide) s in the melt by enantiomeric polymer blending. Polymer 44(10):2891–2896
5. Aou K, Hsu SL, Kleiner LW, Tang F-W (2007) Roles of conformational and configurational defects on the physical aging of amorphous poly (lactic acid). J Phys Chem B 111(42):12322–12327
6. Shen Y, Jing T, Ren W, Zhang J, Jiang Z-G, Yu Z-Z, Dasari A (2012) Chemical and thermal reduction of graphene oxide and its electrically conductive polylactic acid nanocomposites. Compos Sci Technol 72(12):1430–1435
7. Cao Y, Feng J, Wu P (2010) Preparation of organically dispersible graphene nanosheet powders through a lyophilization method and their poly (lactic acid) composites. Carbon 48(13):3834–3839
8. Kim IH, Jeong YG (2010) Polylactide/exfoliated graphite nanocomposites with enhanced thermal stability, mechanical modulus, and electrical conductivity. J Polym Sci, Part B: Polym Phys 48(8):850–858
9. Xu J-Z, Liang Y-Y, Huang H-D, Zhong G-J, Lei J, Chen C, Li Z-M (2012) Isothermal and non-isothermal crystallization of isotactic polypropylene/graphene oxide nanosheet nanocomposites. J Polym Res 19(10):1–7
10. Mohamadi S, Sharifi-Sanjani N, Foyouhi A (2013) Evaluation of graphene nanosheets influence on the physical properties of PVDF/PMMA blend. J Poly Res 20(1):1–10
11. Hajian M, Reisi MR, Koohmareh GA, Jam ARZ (2012) Preparation and characterization of polyvinylbutyral/graphene nanocomposite. J Poly Res 19(10):1–7
12. Lim Y, Tan Y, Lim H, Huang N, Tan W (2013) Preparation and characterization of poly-pyrrole/graphene nanocomposite films and their electrochemical performance. J Poly Res 20(6):1–10
13. Allen MJ, Tung VC, Kaner RB (2010) Honeycomb carbon: a review of graphene. Chem Rev 110(1):132
14. Gopiraman M, Fujimori K, Zeeshan K, Kim B, Kim I (2013) Structural and mechanical properties of cellulose acetate/graphene hybrid nanofibers: spectroscopic investigations. Express Polym Lett 7(6):554–563
15. Celis K, Driessche I, Mouton R, Vanhoyland G, Hoste S (2001) Kinetics of consecutive reactions in the solid state: thermal decomposition of oxalates. Meas Sci Rev 1(1):177–180
16. Vyazovkin S, Burnham AK, Criado JM, Pérez-Maqueda LA, Popescu C, Sbirrazzuoli N (2011) ICTAC Kinetics Committee recommendations for performing kinetic computations on thermal analysis data. Thermochim Acta 520(1):1–19
17. Vyazovkin S, Wight CA (1999) Model-free and model-fitting approaches to kinetic analysis of isothermal and nonisothermal data. Thermochim Acta 340:53–68
18. Saha B, Ghoshal A (2006) Model-free kinetics analysis of waste PE sample. Thermochim Acta 451(1):27–33
19. Chrissafis K (2010) Detail kinetic analysis of the thermal decomposition of PLA with oxidized multi-walled carbon nanotubes. Thermochim Acta 511(1):163–167
20. Li J, Zheng W, Li L, Zheng Y, Lou X (2009) Thermal degradation kinetics of *g*-HA/PLA composite. Thermochim Acta 493(1):90–95
21. Kim HS, Park BH, Choi JH, Yoon JS (2008) Mechanical properties and thermal stability of poly (L-lactide)/calcium carbonate composites. J Appl Polym Sci 109(5):3087–3092
22. Barroso-Bujans F, Alegría A, Pomposo JA, Colmenero J (2013) Thermal stability of polymers confined in graphite oxide. Macromolecules 46(5):1890–1898
23. Seo MK, Park SJ (2004) A kinetic study on the thermal degradation of multi-walled carbon nanotubes-reinforced poly (propylene) composites. Macromol Mater Eng 289(4):368–374
24. Kim SD, Kim JW, Im JS, Kim YH, Lee YS (2007) A comparative study on properties of multi-walled carbon nanotubes (MWCNTs) modified with acids and oxyfluorination. J Fluor Chem 128(1):60–64
25. Schierz A, Zänker H (2009) Aqueous suspensions of carbon nanotubes: surface oxidation, colloidal stability and uranium sorption. Environ Pollut 157(4):1088–1094. doi:10.1016/j.envpol.2008.09.045
26. Ferrari AC (2007) Raman spectroscopy of graphene and graphite: disorder, electron–phonon coupling, doping and nonadiabatic effects. Solid State Commun 143(1):47–57
27. Song P, Cao Z, Cai Y, Zhao L, Fang Z, Fu S (2011) Fabrication of exfoliated graphene-based polypropylene nanocomposites with enhanced mechanical and thermal properties. Polymer 52(18):4001–4010
28. Abuilaiwi FA, Laoui T, Al-Harthi M, Atieh MA (2010) Modification and functionalization of multiwalled carbon nanotube (MWCNT) via Fischer esterification. Arab J Sci Eng 35(1C):37–48
29. Macan J, Brnardić I, Orlić S, Ivanković H, Ivanković M (2006) Thermal degradation of epoxy–silica organic–inorganic hybrid materials. Poly Degrad Stab 91(1):122–127

30. Park S-J, Kim H-C, Lee H-I, Suh D-H (2001) Thermal stability of imidized epoxy blends initiated by *N*-benzylpyrazinium hexafluoroantimonate salt. Macromolecules 34(22):7573–7575
31. Doyle C (1961) Estimating thermal stability of experimental polymers by empirical thermogravimetric analysis. Anal Chem 33(1):77–79
32. Tang W, Li XG, Yan D (2004) Thermal decomposition kinetics of thermotropic copolyesters made from trans-p-hydroxycinnamic acid and p-hydroxybenzoic acid. J Appl Polym Sci 91(1):445–454
33. Paik P, Kar KK (2008) Kinetics of thermal degradation and estimation of lifetime for polypropylene particles: effects of particle size. Polym Degrad Stab 93(1):24–35
34. Kim JY, Kim DK, Kim SH (2009) Thermal decomposition behavior of poly (ethylene 2, 6-naphthalate)/silica nanocomposites. Polym Compos 30(12):1779–1787
35. Nabipour Chakoli A, Wan J, Feng JT, Amirian M, Sui JH, Cai W (2009) Functionalization of multiwalled carbon nanotubes for reinforcing of poly (l-lactide-co-ε-caprolactone) biodegradable copolymers. Appl Surf Sci 256:170–177
36. Doyle C (1962) Estimating isothermal life from thermogravimetric data. J Appl Polym Sci 6(24):639–642
37. Doyle C (1961) Kinetic analysis of thermogravimetric data. J Appl Polym Sci 5(15):285–292
38. Flynn J (1983) The isoconversional method for determination of energy of activation at constant heating rates. J Therm Anal Calorim 27(1):95–102
39. Cooney J, Day M, Wiles D (1983) Thermal degradation of poly (ethylene terephthalate): a kinetic analysis of thermogravimetric data. J Appl Polym Sci 28(9):2887–2902
40. Kim H-S, Hyun Park B, Yoon J-S, Jin H-J (2007) Thermal and electrical properties of poly (L-lactide)-graft-multiwalled carbon nanotube composites. Eur Polym J 43(5):1729–1735
41. Wang FY, Ma CCM, Wu WJ (2001) Kinetic parameters of thermal degradation of polyethylene glycol-toughened novolac-type phenolic resin. J Appl Polym Sci 80(2):188–196
42. Coats A, Redfern J (1964) Kinetic parameters from thermogravimetric data. Nature 201:68–69
43. Cai J, Yao F, Yi W, He F (2006) New temperature integral approximation for nonisothermal kinetics. AIChE J 52(4):1554–1557
44. Carrasco F, Pérez-Maqueda LA, Sánchez-Jiménez P, Perejón A, Santana O, Maspoch ML (2013) Enhanced general analytical equation for the kinetics of the thermal degradation of poly (lactic acid) driven by random scission. Polym Test 32(5):937–945
45. Aoyagi Y, Yamashita K, Doi Y (2002) Thermal degradation of poly [(*R*)-3-hydroxybutyrate], poly [ε-caprolactone], and poly [(*S*)-lactide]. Polym Degrad Stab 76(1):53–59
46. Sheiko SS, Sun FC, Randall A, Shirvanyants D, Rubinstein M, Lee H-I, Matyjaszewski K (2006) Adsorption-induced scission of carbon–carbon bonds. Nature 440(7081):191–194